CHEM**CAT**CHEM

Supporting Information

Assessment of the Location of Pt Nanoparticles in Pt/zeolite Y/γ-Al₂O₃ Composite Catalysts

Jogchum Oenema, Jan P. Hofmann, Emiel J. M. Hensen, Jovana Zečević,* and Krijn P. de Jong*

Supporting Information

Assessment of the location of Pt nanoparticles in Pt/zeolite Y /γ-Al$_2$O$_3$ composite catalysts

Jogchum Oenema[a], Jan P. Hofmann[b], Emiel J. M. Hensen[b], Jovana Zečević*[a], and Krijn P. de Jong*[a]

[a]   Inorganic Chemistry and Catalysis, Debye Institute for Nanomaterials Science, Utrecht University, Universiteitsweg 99, 3584 CG Utrecht, The Netherlands.

[b]   Laboratory for Inorganic Materials and Catalysis, Department of Chemical Engineering and Chemistry, Eindhoven University of Technology, P.O. Box 513, 5600 MB Eindhoven, The Netherlands.

* E-mail: J.Zecevic@uu.nl, K.P.dejong@uu.nl

Table of Contents

Table S1. Employed characterization techniques with the investigated area, corresponding studied volume and the mass of the material studied.

Technique	Sampled area	Sampling depth	Total studied sample volume (m^3)	Total studied sample mass (g)
TEM	Field of view: 200 nm × 200 nm	Sample thickness: 70 nm	$2.8 \cdot 10^{-21}$	$\sim 10^{-14}$
Quantitative XPS	X-ray spot size: 400 μm ø	EMFP: 1-5 nm	10^{-16}-10^{-15}	$\sim 10^{-9}$
CO infrared spectroscopy	Weight of pellet determined on an analytical balance			$\sim 10^{-2}$
Catalysis	Weight of catalyst determined on an analytical balance			$5 \cdot 10^{-2}$

Supporting information 1.1

TEM

The field of view of a typical high magnification TEM image is 200 x 200 nm and the microtomed samples have a thickness of 70 nm. We assume that the field of view of the TEM is completely filled with sample and therefore the studied volume of sample per image corresponds to $2.8 \cdot 10^{-21}$ m^3. The highly porous metal oxide supports used in this study have a density in the order of 10^6 $g \cdot m^{-3}$, and thus the amount of material studied is in the range of 10^{-15}-10^{-14} g per TEM image. For TEM measurements commonly multiple TEM images are made of different areas of the sample, increasing the total amount of studied material by 1, or maximally 2 orders of magnitude.

Quantitative XPS

For the XPS measurements, a monochromatic Al Kα source of hv = 1486.6 eV was used and therefore the kinetic energy of Pt 4f photoelectrons will be in the range of 1410-1415 eV, while kinetic energies for Al 2s, Al 2p, Si 2p core levels will be between 1360-1415 eV. The escape depth of photoelectrons (with a kinetic energy in the range of 1360-1415 eV) for metal oxide supports is between 1-5 nm (see SI section 1.2).[1,2] For the XPS measurements a spot size of 400 µm diameter was used corresponding to an X-ray irradiated area of $1.3 \cdot 10^{-7}$ m^2 and therefore the sampled volume is in the order of 10^{-16}-10^{-15} m^3 per measurement. Assuming a typical porous metal oxide density in the order of 10^6 $g \cdot m^{-3}$ will give a sampled amount of material in the range of 10^{-10}-10^{-9} g, which is multiple orders of magnitude more than what is sampled in a typical TEM experiment. Performing multiple measurements at different locations on the sample can further increase the amount of sampled material (for this study 2 locations were measured).
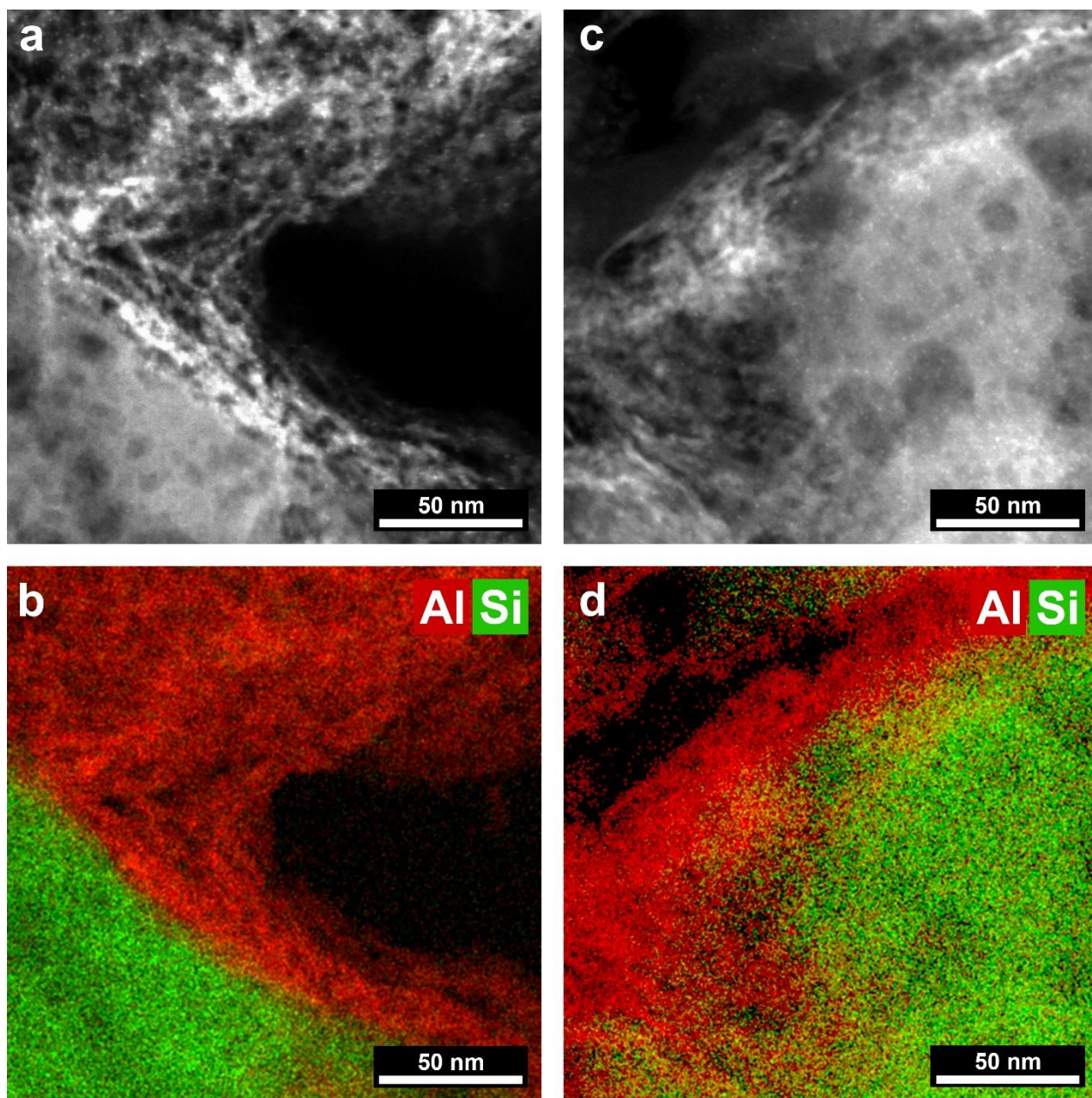
Figure S1. HAADF-STEM images of microtomed sections of Pt-Y/A-Cl (a) where Pt nanoparticles (apparent as bright white spots) are located on the γ-Al$_2$O$_3$ component, corresponding to the red region in the EDX elemental map (b) of the same area. HAADF-STEM images of microtomed sections of Pt-Y/A-NH$_3$ (c) with Pt nanoparticles located in the zeolite Y that can be identified as the green region in the EDX elemental map (d) of the same area.
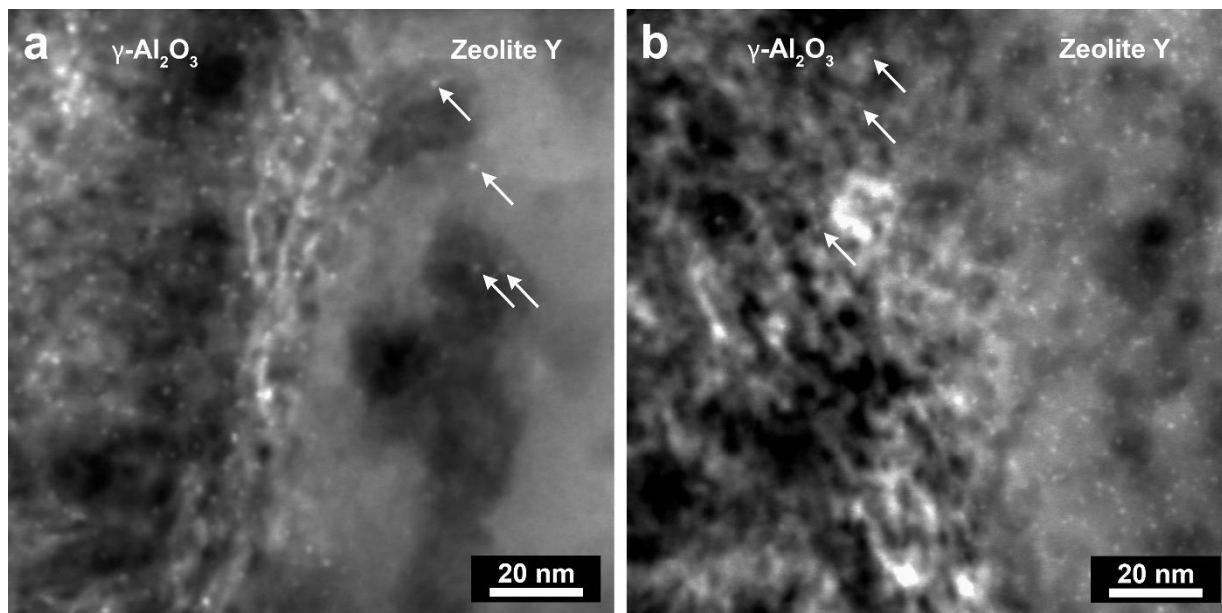
Figure S2. HAADF-STEM images of microtomed sections of Pt-Y/A-Cl (a) and Pt-Y/A-NH$_3$ (b) with the zeolite Y and γ-Al$_2$O$_3$ components indicated in the. The ~1.5 nm Pt nanoparticles can be identified as white dots, almost exclusively present in the γ-Al$_2$O$_3$ for Pt-Y/A-Cl (a) and almost exclusively present in zeolite Y for Pt-Y/A-NH$_3$ (b). White arrows indicate Pt nanoparticles that are located close to the interface of zeolite Y and γ-Al$_2$O$_3$ and that could be located on the 'opposite' component but difficult to determine unequivocally.

Figure S3. Histogram showing the size distribution of Pt nanoparticles of Pt-Y/A-Cl and Pt-Y/A-NH$_3$ as obtained from measuring individual particles on HAADF-STEM images. For Pt-Y/A-Cl 268 particles were counted, for Pt-Y/A-NH$_3$ 379 particles.
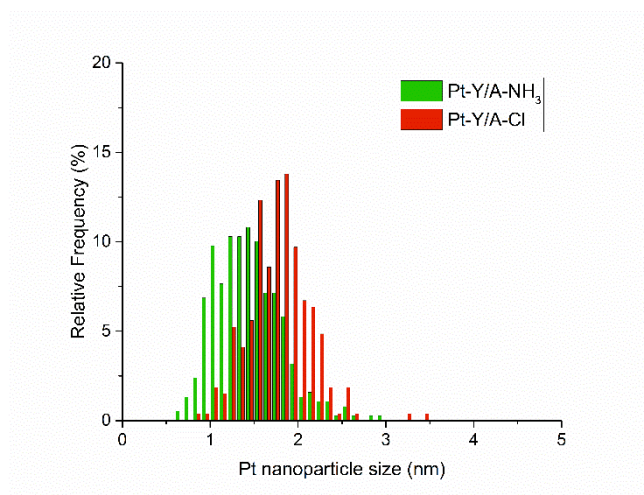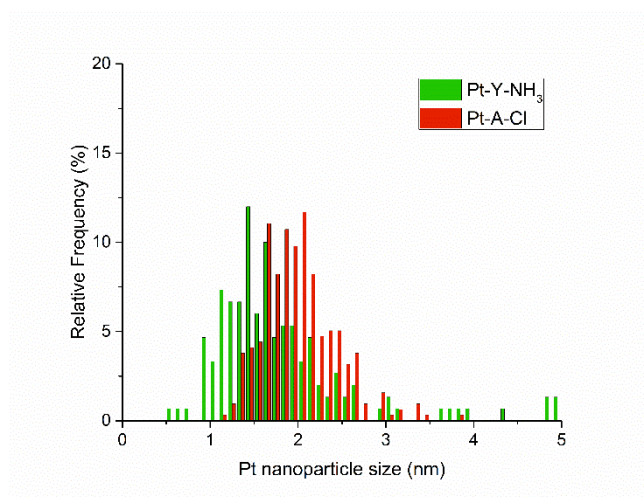

Figure S4. Histogram showing the size distribution of Pt nanoparticles of Pt-A-Cl and Pt-Y-NH$_3$ as obtained from measuring individual particles on HAADF-STEM images. For Pt-A-Cl 317 particles were counted, for Pt-Y/A-NH$_3$ 162 particles.
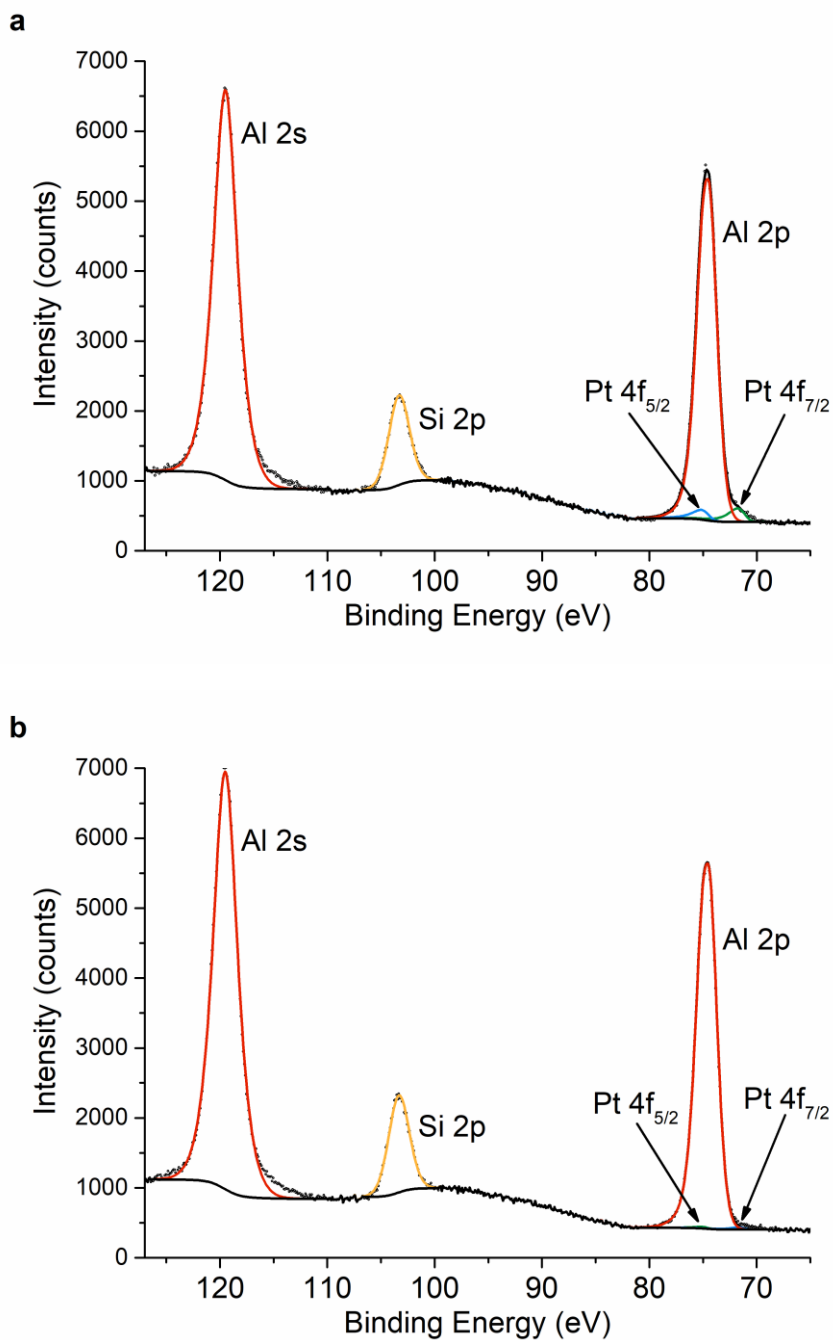
Figure S5. The high resolution XPS regional spectra showing the Al 2s. Si 2p, Al 2p, and Pt 4f core levels of Pt-Y/A-Cl (a) and Pt-Y/A-NH$_3$ (b). XPS data is depicted with small black circles. Color scheme: Pt 4f$_{5/2}$ (light blue), Pt 4f$_{7/2}$ (dark green), Al 2p and Al 2s (red), Si 2p (orange), Shirley background and overall fit (black).

Table S2. Summary of XPS results of measurements on catalyst samples and reference measurements used for spectra quantification, combined with Pt wt.%, bulk atomic ratios for Pt from ICP and manufacturers specification for Si and Al. Pt particle size was obtained from TEM analysis. Standard deviation for Pt nanoparticle sizes was based on the deviation in measuring 162-379 Pt nanoparticles from TEM images. The standard deviation in XPS measurements indicated here was based on results of two measurements on different spots on the sample. The bulk atomic ratio for physical mixtures are based on the amount of each compound used for the physical mixture, determined by weighing the powders on a analytical balance.

Sample	Pt wt.%	d_{Pt} (nm)	Bulk (at/at)		Surface (at/at)	
			Si/Al	Pt/Al	Si/Al	Pt/Al
Composite catalyst						
Pt-Y/A-NH$_3$	0.47	1.4 ± 0.4	0.80	0.0024	0.176 ± 0.001	0.0003 ± 0.0001
Pt-Y/A-Cl	0.48	1.8 ± 0.4	0.80	0.0025	0.182 ± 0.009	0.0021 ± 0.0003
Physical mixtures						
Pt-Y-NH$_3$ + A	0.47	2.2 ± 1.6	0.78	0.0024	0.79 ± 0.01	0.00015 ± 0.00003
Pt-A-Cl + Y	0.52	1.5 ± 0.3	0.69	0.0025	0.827 ± 0.004	0.0009 ± 0.0002
Pt on single component supports						
Pt-Y-NH$_3$	0.95	2.2 ± 1.6	30	0.0911	17 ± 3	0.0034 ± 0.0002
Pt-A-Cl	0.97	1.5 ± 0.3	-	0.0026	-	0.0023 ± 0.0001
Supports						
Y/A	-	-	0.80	-	0.199 ± 0.005	-
Y (Zeolite Y)	-	-	30	-	21 ± 6	-
A (γ-Al$_2$O$_3$)	-	-	-	-	-	-

Supporting Information 1.2

Experimental details XPS measurements

Prior to the XPS measurements, the catalysts grains were mortared to a fine powder to increase the surface to volume ratio of the sample. In all samples elements C, O, Al, Si, Pt are present. Some samples contain small amounts of Cl. Two spots per sample have been measured. Binding energy calibration was done by setting the C 1s binding energy of the adventitious carbon CC/CH (sp^3) peak to 284.8 eV. The presence of Pt next to Al complicates analysis due to the overlapping main core levels Al 2p and Pt 4f. From survey spectra, a quantitative analysis is thus not possible. Region scans have been taken for all samples covering the core levels Pt 4f / Al 2p, Si 2p and Al 2s. The area of the Al 2p peak was put into ratio with the area of the Al 2s for a reference pure Al_2O_3 sample. The same ratio has been applied to the Pt/zeolite Y/γ-Al_2O_3 samples and reference samples provided in Table S2, to determine the area of the Al 2p in the overlapping Pt 4f / Al 2p region based on the fitting of the isolated Al 2s peak. The remaining area was then fitted to two components with asymmetric (metallic) line shape for Pt 4f$_{5/2}$ and Pt 4f$_{7/2}$ core levels, whereas the line shape function, the FWHM were kept identical for both peaks of the spin-orbit split doublet and the S-O splitting was fixed to 3.35 eV. The BE of Pt 4f$_{7/2}$ ranges between 71.1-71.5 eV, indicating metallic Pt. The isolated Pt 4d core level is much weaker and could not be used for quantification due to the low amounts of Pt present in the samples.

The intensities of Pt 4f core levels for Pt-Y/A-NH$_3$ and Pt-Y-NH$_3$ + A are close to the detection limit that results in a large relative error in Pt/Al ratio. By manually altering the constraints used during the fitting of the spectra, changes of +/- 100% in the fitted Pt 4f area of Pt-Y/A-NH$_3$ and Pt-Y-NH$_3$ + A could be introduced. For Pt-Y/A-Cl and Pt-A-Cl + Y, samples with higher Pt/Al ratio's, such variations were not observed upon altering the constraints.

Electron Mean Free Path (EMFP) in γ-Al$_2$O$_3$

Literature data of Al$_2$O$_3$ and SiO$_2$.

	Solid density (g/cm^3), Ref:[3]	EMPF in bulk solids E_{kin} = 1415 eV (nm), Ref:[2]
Al$_2$O$_3$	3.65	1.8
SiO$_2$	2.196[a]	2.6

a) density of fused silica.

In this case, Pt 4f, Al 2p and Si 2p photoelectrons are studied with a kinetic energy of 1380-1420 eV that need to emit from samples that consist of zeolite Y and γ-Al$_2$O$_3$ that have very different morphology and composition. γ-Al$_2$O$_3$ consists of an irregular platelet like structure with high surface to volume ratio that can be approximated as infinite sheets as has been proposed by Kerkhof et al.[4]

$$t_s = \frac{2}{\rho_s \cdot \sigma_s} = \frac{2}{314 \, m^2 \cdot g^{-1} \cdot 3.65 \cdot 10^6 \, g \cdot m^{-3}} = 1.8 \, nm$$

The approximated γ-Al$_2$O$_3$ sheet thickness is similar to the EMFP in bulk Al$_2$O$_3$ (1.8 nm) and therefore the Pt XPS signal of Pt nanoparticles located on γ-Al$_2$O$_3$ will mainly consist of contributions of Pt nanoparticles located on the surface of externally oriented γ-Al$_2$O$_3$ platelets, with minor contributions from Pt nanoparticles underneath the γ-Al$_2$O$_3$ surface layer.

Electron Mean Free Path (EMFP) in zeolite Y

The zeolite Y crystallites of the zeolite Y/γ-Al$_2$O$_3$ composite support are a steamed and acid leached derivative of Na-zeolite Y (Zeolyst CBV100) that consists of large crystallites of 200-1000 nm in size and a corresponding small external surface area of ~8 m^2/g.[5] In order to correct for the

effect of zeolite microporosity on the EMFP, the void fraction in zeolite Y is determined by using the zeolite Y micropore volume from N_2 physisorption using the t-plot method.

The void fraction of zeolite Y is given by:

$$\phi_{\text{zeolite Y}} = \frac{\rho_{SiO2} \cdot V_{zeolite\ Y}}{1 + \rho_{SiO2} \cdot V_{zeolite\ Y}} = \frac{2.20\ g \cdot cm^{-3} \cdot 0.28\ cm^3 \cdot g^{-1}}{1 + 2.20\ g \cdot cm^{-3} \cdot 0.28\ cm^3 \cdot g^{-1}} = 0.38$$

Using the EMFP of silica (Table S3), the electron mean free path in zeolite Y is then given by:

$$EMFP_{zeolite\ Y} = \frac{EMFP_{SiO2}}{1 - \phi} = \frac{2.6\ nm}{1 - 0.38} \approx 4\ nm$$

Stakheev et al. has previously reported a void fraction of 0.47, based on the water content of hydrated faujasite, resulting in an apparent EMFP of ~5 nm, which corresponds to the first two or three unit cells (2.5 nm) of zeolite Y subjacent the external surface.[6,7]
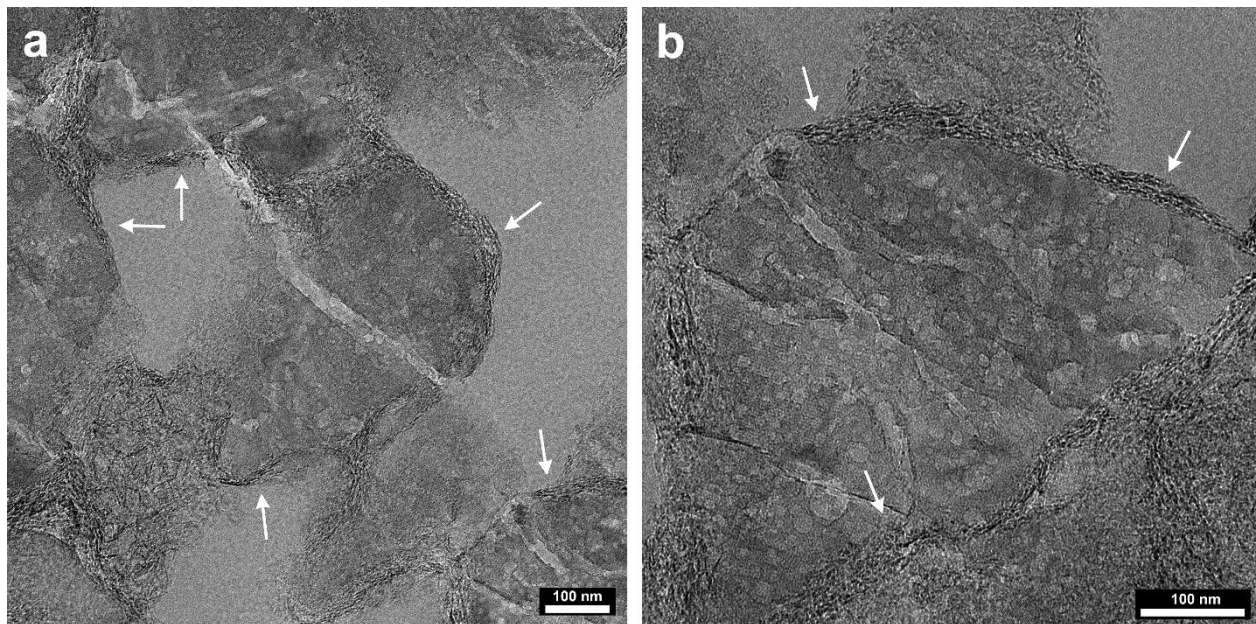
Figure S6. Bright-field TEM images (a,b) of ~70 nm microtome-cut sections at different magnifications showing the Y/A support. Zeolite Y crystals are coated with a layer of γ-Al$_2$O$_3$, as indicated by arrows. The γ-Al$_2$O$_3$ can be identified by the typical acicular (needle-like) morphology while zeolite Y consists of mesoporous crystallites between 200-1000 nm in size.
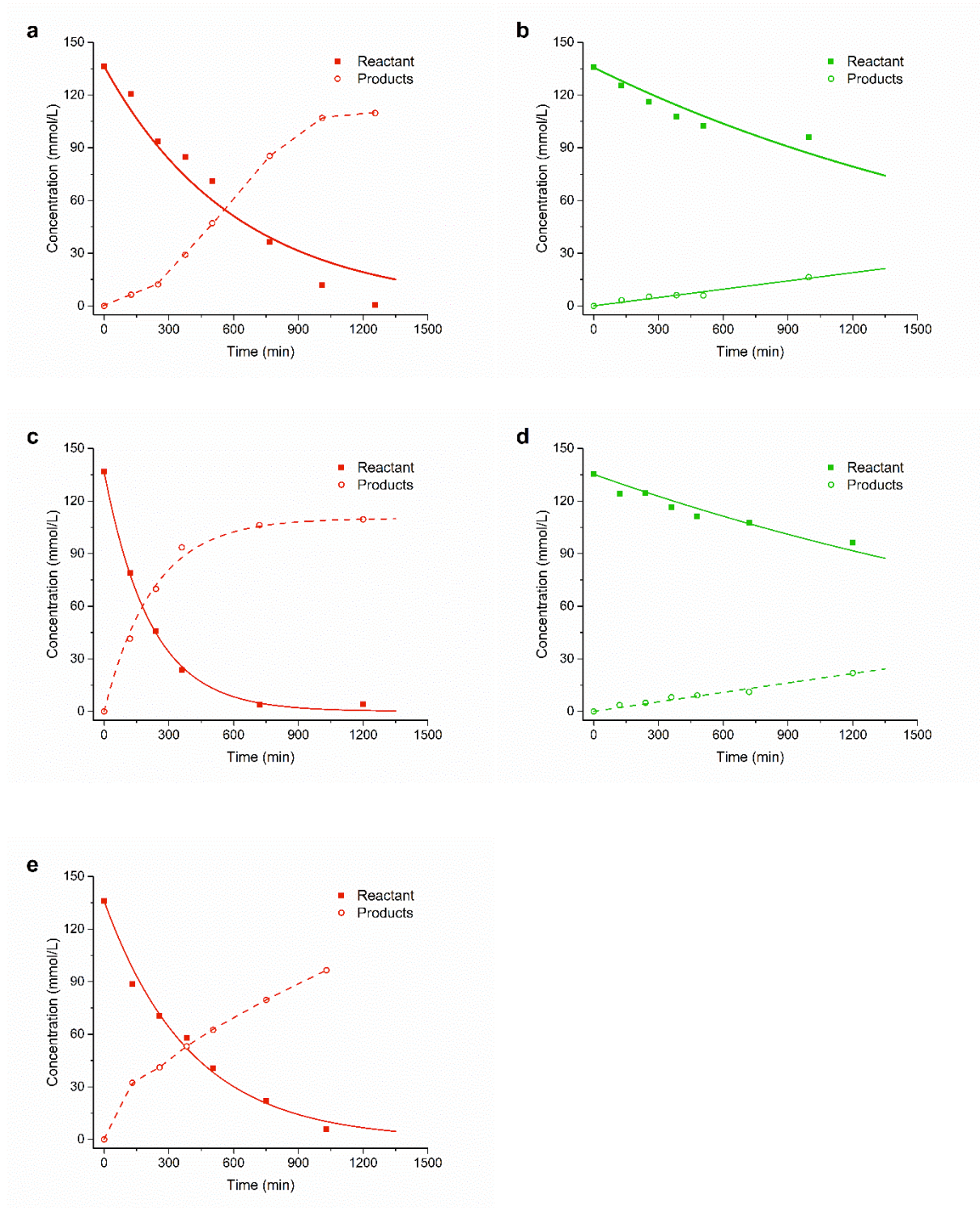
Figure S7. Reaction profiles showing concentrations of BPCMA (filled symbols) and Products (open symbols) as a function of time. Solid lines are first order kinetic fits of BPCMA as reactant

concentration, dotted lines indicate the concentration of products and are added to guide the eye. Catalysts: Pt-Y/A-Cl (a), Pt-Y/A-NH$_3$ (b), Pt-A-Cl (c). Pt-Y-NH$_3$ (d) and Pt-A-Cl + Y (e).

Table S3. The weight based rate constant was obtained by fitting the concentration profiles to first-order kinetics (normalized to the amount of Pt per unit volume in the reactor), using close to identical initial concentrations of BPCMA. The Pt loading of the catalysts was determined by ICP, whereas the initial concentration of BPCMA was obtained by weighing the reactant on an analytical balance. The mass balance of the reaction (sum of products an reactants divided by amount of reactant at t=0) as obtained by GC analysis is also reported.

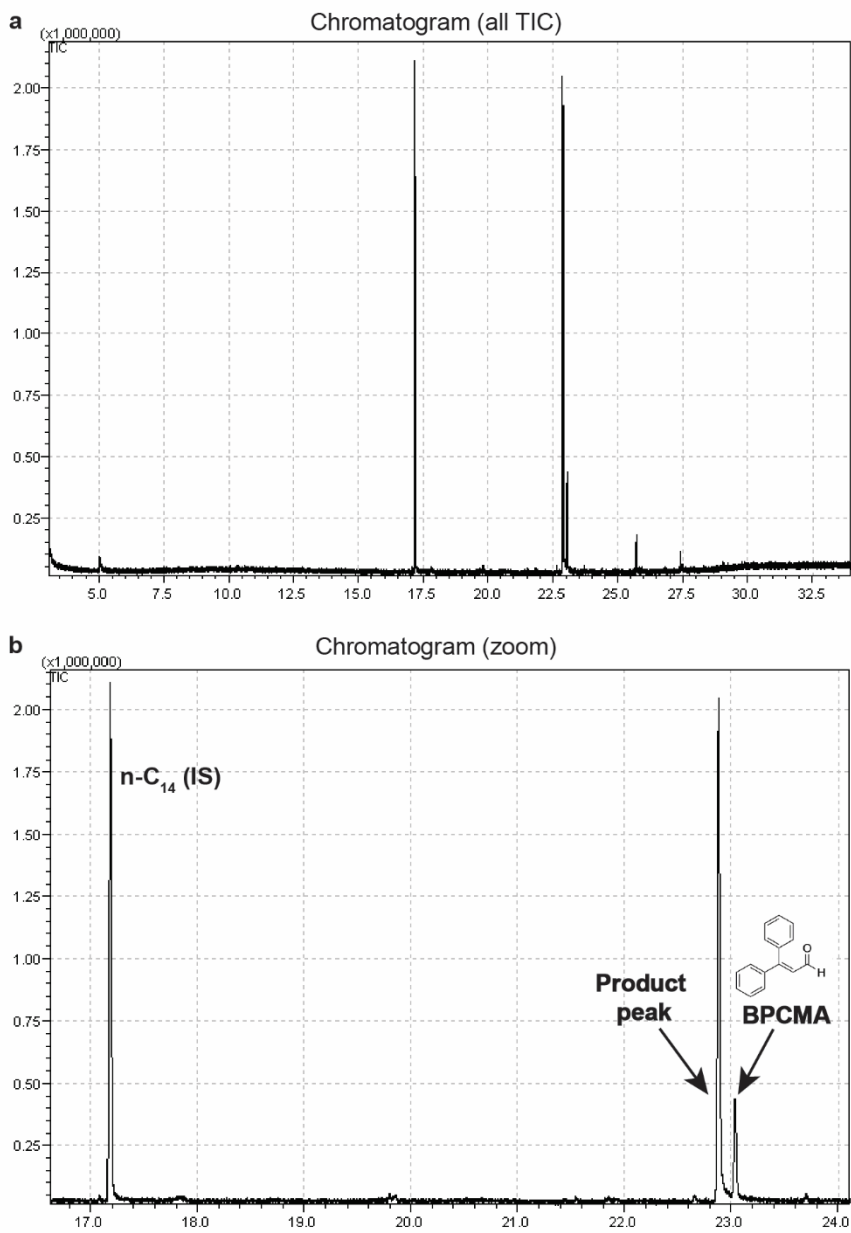|	Pt. loading (wt.%)	$C_{t=0}$ (mmol/l)	k_w (ml·g$_{Pt}^{-1}$·s^{-1})	Mass balance (%)
Pt-Y/A-Cl	0.3	136	3.0	81
Pt-Y/A-NH$_3$	0.4	136	0.6	83
Pt-A-Cl	0.7	137	6.4	83
Pt-Y-NH$_3$	0.8	135	0.4	87
Pt-A-Cl + Y	0.4	137	3.5	81

Figure S8. The full (a) or zoomed (b) GC-MS chromatogram of a sample taken from reaction mixture after 360 minutes with the Pt-A-Cl catalyst. Chromatograms show separate peaks for BPCMA and the formed product.
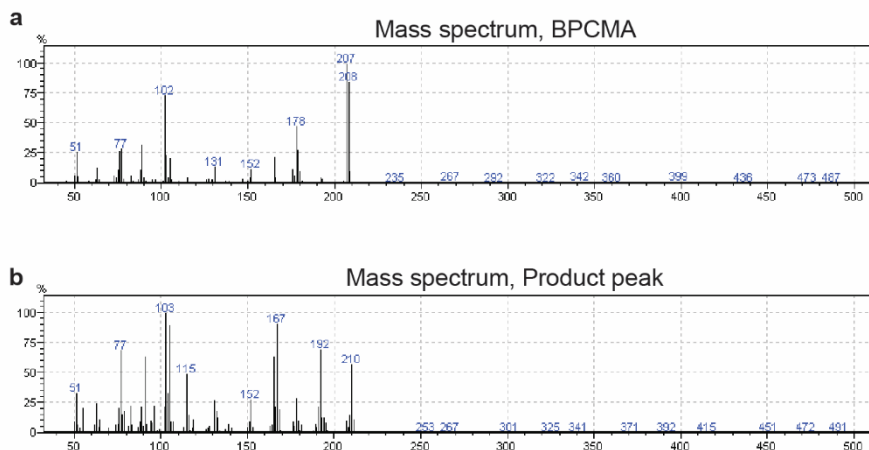
Figure S9. Mass spectra with peaks corresponding to BPCMA (a) and the mass spectra corresponding to the product peak (b). BPCMA and the formed products are not available in the NIST database. From the fragmentation in the MS spectrum it is apparent that the predominant product is an alcohol derivative of BPCMA, whereby the carbonyl group is converted into a hydroxyl group.
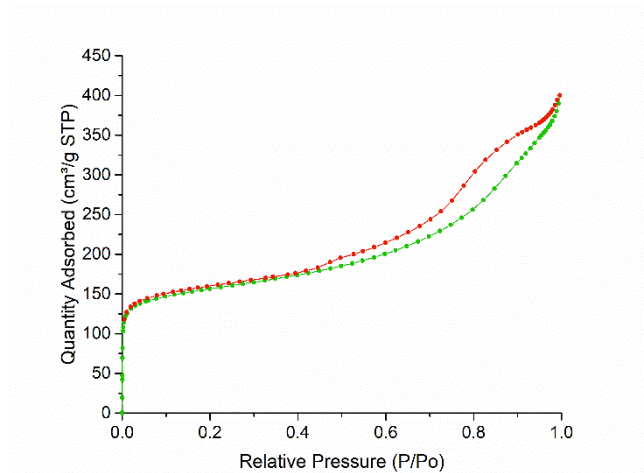
Figure S10. N_2 physisorption isotherms of the Y/A (zeolite Y/γ-Al_2O_3) composite support.
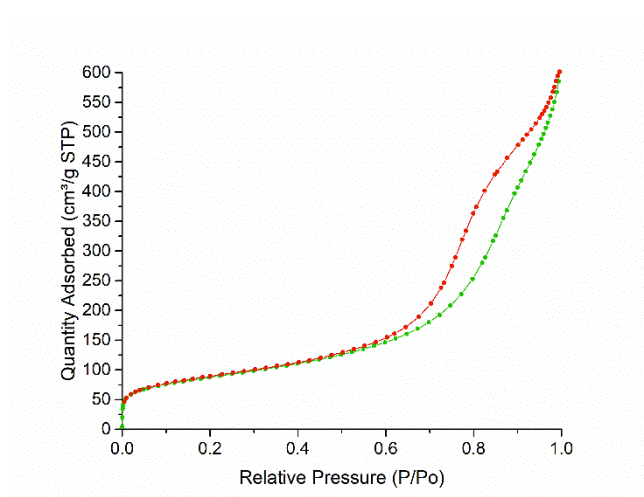

Figure S11. N_2 physisorption isotherms of the bare A (γ-Al_2O_3) binder. The γ-Al_2O_3 was prepared by calcination of pseudo-boehmite at 550°C (2h, 5°C/min,)

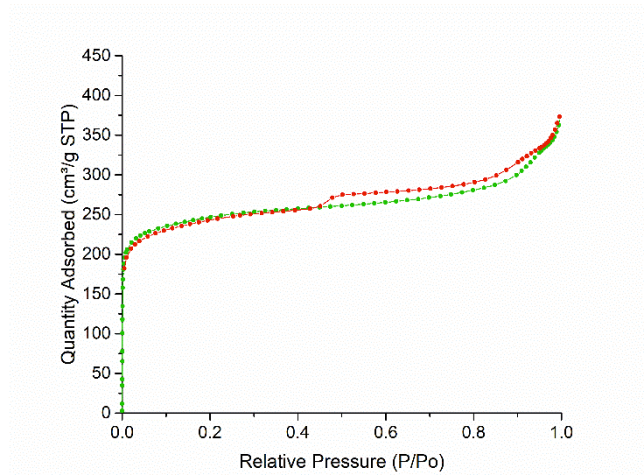**Figure S12.** N_2 physisorption isotherms of the zeolite Y (Zeolyst CBV760).

Table S4. Results of textural analysis of the Y/A composite support and single components.

	BET surface area (m^2/g)	BJH pore volume (cm^3/g)	t-plot micropore volume (cm^3/g)	t-plot external surface area(m^2/g)
Y/A	-	0.44	0.15	209
A (γ-Al_2O_3)	314	0.89	0.02	294
Y (zeolite Y)	-	0.24	0.28	231

References

[1] M. P. Seah, W. A. Dench, Surf. Interface Anal. 1979, 1, 2–11.

[2] T. Reich, V. G. Yarzhemski, V. I. Nefedov, J. Electron Spectros. Relat. Phenomena 1988, 46, 255–267.

[3] J. Rumble, Ed. , Handbook of Chemistry and Physics, CRC Press/Taylor & Francis, Boca Raton, FL., 2018.

[4] F. P. J. M. Kerkhof, J. A. Moulijn, J. Phys. Chem. 1979, 83, 1612–1619.

[5] A. H. Janssen, A. J. Koster, K. P. de Jong, Angew. Chemie Int. Ed. 2001, 40, 1102–1104.

[6] A. Y. Stakheev, W. M. H. Sachtler, J. Chem. Soc. Faraday Trans. 1991, 87, 3703–3708.

[7] T. L. Barr, M. A. Lishka, J. Am. Chem. Soc. 1986, 108, 3178–3186.